JOC Article

Electrocyclic Ring Opening of Charged *cis*-Bicyclo[3.2.0]heptadiene and Heterocyclic Derivatives. The Anti-Woodward−Hoffmann Quest (II)[1]

Carlos Silva López,* Olalla Nieto Faza, and Ángel R. de Lera*

Departamento de Química Orgánica, Facultade de Química, Universidade de Vigo, Lagoas Marcosende, 36310, Vigo, Galicia, Spain

csilval@uvigo.es; qolera@uvigo.es

Received December 9, 2008

Ⓦ **This paper contains enhanced objects available on the Internet at http://pubs.acs.org/joc.**

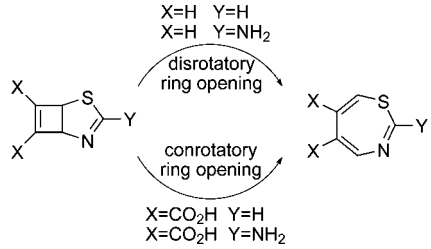

The ring opening reactions of fused cyclobutenes have been the subject of mechanistic debate for decades. Some reports have been published recently suggesting that, in some heterocyclic derivatives, the disrotatory anti-Woodward−Hoffmann mechanism might be responsible for the ring opening. We hereby show that the conrotatory pathway is still the lowest energy alternative for all cases examined, including push−pull substituted 2-thia-4-azabicyclo[3.2.0]hepta-3,6-dienes. Actually, we found that the disrotatory transition state exchanges roles with a double-bond isomerization depending on the substituents around the bicyclic structure.

1. Introduction

Woodward and Hoffmann's most relevant contribution to chemistry has demonstrated over the decades its robustness, predictive power, and versatility in such great extent that it has become one of the cornerstones on which modern organic chemistry rests.[2,3] The near infallibility of the Woodward−Hoffman (W−H) rules has impelled chemists to explore and define its frontiers. For years, the anti-W−H quest has failed in numerous occasions due, mainly, to two reasons. First, the seemingly forbidden reaction can actually proceed in a stepwise fashion where an allowed concerted process occurs to furnish a short living intermediate, which is subsequently transformed into the apparent anti-W−H product.[4] Second, the proposed forbidden reaction proceeds via diradical[5] or zwitterionic[6] species, circumventing the W−H rules.

We recently explored computationally the cycloisomerization of *cis*-bicyclo[4.2.0]oct-7-ene, whose mechanism has been a subject of debate for decades (Figure 1).[7−9] We concluded that the reaction proceeded via the allowed conrotatory electrocyclic ring opening of the fused cyclobutene to yield an intermediate which rapidly undergoes a *trans-cis* double-bond isomerization leading to the observed *cis,cis*-1,3-cyclooctadiene. A thorough study on analogous systems was also conducted in which the effect of ring strain in the series *cis*-bicyclo[4.2.0]oct-7-ene (**A**), *cis*-bicyclo[3.2.0]hept-6-ene (**B**), *cis*-bicyclo[2.2.0]hex-2-ene (**C**), and *cis*-bicyclo[2.1.0]pent-2-ene (**D**) was explored (Figure 1).[10] The frontier where the W−H allowed and forbidden electrocyclic ring opening reactions meet

(1) This work extends a thorough study on the ring opening of fused cyclobutenes[10] and adds insight into the effect of hetero-substitution at key positions of the molecular scaffold.

(2) Woodward, R. B.; Hoffmann, R. *J. Am. Chem. Soc.* **1965**, *87*, 395–397.

(3) Wilkinson, S. *Chem. Eng. News* **2003**, *81* (4), 59.

(4) Faza, O. N.; López, C. S.; Álvarez, R.; de Lera, A. R. *Org. Lett.* **2004**, *6*, 901–904.

(5) Davidson, E. R.; Gajewski, J. J.; Shook, C. A.; Cohen, T. *J. Am. Chem. Soc.* **1995**, *117*, 8495–8501.

(6) Guimares, C. R. W.; Udier-Blagovi, M.; Jorgensen, W. L. *J. Am. Chem. Soc.* **2005**, *127*, 3577–3588.

(7) López, C. S.; Faza, O. N.; de Lera, A. R. *Org. Lett.* **2006**, *8*, 2055–2058.

(8) Baldwin, J. E.; Gallagher, S. S.; Leber, P. A.; Raghavan, A. *Org. Lett.* **2004**, *6*, 1457–1460.

(9) Baldwin, J. E.; Gallagher, S. S.; Leber, P. A.; Raghavan, A. S.; Shukla, R. *J. Org. Chem.* **2004**, *69*, 7212–7219.

(10) López, C. S.; Faza, O. N.; de Lera, A. R. *Chem. Eur. J.* **2007**, *13*, 5009–5017.

10.1021/jo802678d CCC: $40.75 © 2009 American Chemical Society
Published on Web 02/16/2009

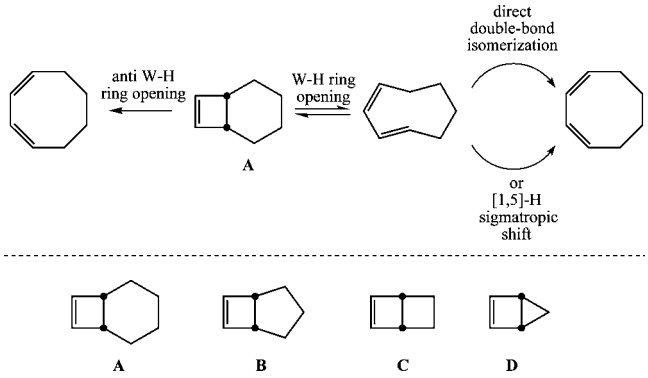

FIGURE 1. Mechanistic alternatives for the ring-opening of *cis*-bicyclo[4.2.0]oct-7-ene **A** to *cis,cis*-1,3-cyclooctadiene (top).[8,9] Previously studied series of fused cyclobutene molecules (bottom).[10]

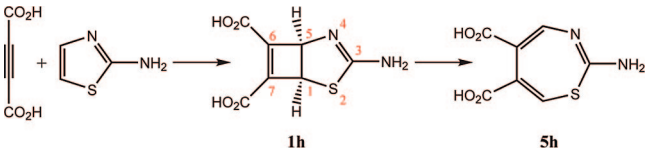

FIGURE 2. Thermal disrotatory ring opening of 3-amino-6,7-dicarboxy-2-thia-4-azabicyclo[3.2.0]hepta-3,6-diene **1h** to *cis,cis,cis*-2-amino-5,6-dicarboxy-1,3-thiazepine **5h**, as proposed in previous work.[11]

was thus delimited with respect to the ring size and found to lie at **C**: larger systems clearly undergo a conrotatory opening, whereas the smaller bicyclic hydrocarbon **D** rearranges only via the formally symmetry-forbidden disrotation through transition states exhibiting strongly diradicaloid character.

Almost concurrently with the submission of our results, a heterocyclic analogue of **B**, **1h**, was reported to seemingly undergo cycloisomerization via a forbidden thermal disrotatory electrocyclic ring opening based on a computational study (see Figure 2).[11]

Intrigued by these computational results, we decided to reproduce them in our laboratory. As expected, the transition structure previously reported was identified as a converged first-order saddle point. However, careful inspection of the normal mode associated with the imaginary frequency revealed that this transition state displayed an unclear motion. We, therefore, decided to conduct a thorough revision on the thermal ring opening of *cis*-bicyclo[3.2.0]hept-6-ene, in particular the role played by heteroatoms and substituents in key positions.

2. Computational Methods

2.1. Geometries and Energy. The density functional theory[12] in its Kohn−Sham[13] formulation was employed for all calculations. The three parameter hybrid functional B3LYP[14−16] was used throughout this work together with a double-ζ basis set with diffuse and polarization functions on heavy atoms, 6-31+G(d). This is the same level of theory employed by Alajarín and co-workers in their study.[11] All the calculations were performed with the Gaussian03 suite.[17]

The broken-symmetry version of B3LYP was used in several calculations since some of the intermediates along the potential reaction mechanism exhibit a strong diradical character. Hybrid density functionals are known to mimic the effect of nondynamic correlation needed to correctly describe diradical (or near degenerate) character, due to the self-interaction error introduced in the local exchange part of the functionals.[18] In our thorough study on the electrocyclic ring opening of fused cyclobutenes, we compared B3LYP to multiconfiguration and multireference methods and concluded that it provides excellent results for this class of reactions.[10] To ensure the validness of the computed data, a stability check of the wave function[19] was performed for all computed stationary points. Analytical frequencies were also computed for all the optimized geometries at the corresponding level of theory. Intrinsic reaction coordinate (IRC) calculations[20,21] were performed for all transition states optimized at the B3LYP/6-31+G(d) level to ensure that the saddle points located actually connected reactants and products or intermediates in the potential energy surface.

2.2. Properties. In order to evaluate the aromatic character of several transition structures, the nucleus-independent chemical shift (NICS)[22] and the anisotropy of the current-induced density (ACID)[23,24] were computed using the gauge-independent atomic orbitals (GIAO)[25] and the continuous set of gauge transformations (CSGT),[26] respectively.

2.3. Transition States. This work aims to establish which mechanistic alternative, W−H or anti-W−H, is more energetically favorable for the ring opening of a series of fused cyclobutenes. Since the W−H alternative involves a seven-membered ring intermediate sporting a *trans* double-bond, a subsequent isomerization step is required to furnish the final product. Along these lines, it was found that, in several cases, the disrotatory transition state and the double-bond isomerization transition state lie very close in the configuration space. For some substrates, this proximity makes one of the transition states vanish. For every such example, a number of different strategies[27] were carried out to explore the potential energy surface and confirm that the transition state reported is the only one to be found in that region.

3. Results and Discussion

3.1. Molecular Scaffold. 3.1.1. Reaction Energetics. The reaction triggering the present study, **1h→5h** (Figure 2), was experimentally performed and computationally explored with a substrate fully adorned with heteroatoms on the bicyclic backbone, electron-withdrawing group at the cyclobutene moiety, and an electron-donor amine forming an isothiourea group on the five-membered ring. We, therefore, decided to conduct our study in a systematic way by starting with a simple molecular scaffold to which complexity is added until the fully substituted compound is built. With this approach, we expected to be able to partition the different contributions to the reactivity of the final substrate **1h** in terms of its structural characteristics (see Figure 3).

Table 1 summarizes the energy profiles for the disrotatory and conrotarory ring opening processes of **1a**−**1e**. **1a**, the

(11) Alajarín, M.; Cabrera, J.; Pastor, A.; Sánchez-Andrada, P.; Bautista, D. *J. Org. Chem.* **2006**, *71*, 5328–5339.
(12) Hohenberg, P.; Kohn, W. *Phys. Rev.* **1964**, *136*, B864−B871.
(13) Kohn, W.; Sham, L. *Phys. Rev. A* **1965**, *140*, A1133–A1138.
(14) Becke, A. D. *Phys. Rev. A* **1988**, *38*, 3098–3100.
(15) Becke, A. D. *J. Chem. Phys.* **1993**, *98*, 5648–5652.
(16) Lee, C.; Yang, W.; Parr, R. G. *Phys. Rev. B* **1988**, *37*, 785–789.
(17) Frisch, M. J. et al. *Gaussian 03, Revision C.02*; Gaussian, Inc.: Wallingford, CT, 2004.
(18) Cremer, D. *Mol. Phys.* **2001**, *99*, 1899–1940.
(19) Bauernschmitt, R.; Ahlrichs, R. *J. Chem. Phys.* **1996**, *22*, 9047–9052.
(20) Gonzalez, C.; Schlegel, H. B. *J. Chem. Phys.* **1989**, *90*, 2154–2161.
(21) Gonzalez, C.; Schlegel, H. B. *J. Phys. Chem.* **1990**, *94*, 5523–5527.
(22) Schleyer, P. v. R.; Maerker, C.; Dransfeld, A.; Jiao, H.; Hommes, N. J. R. v. *J. Am. Chem. Soc.* **1996**, *118*, 6317–6318.
(23) Herges, R.; Geuenich, D. *J. Phys. Chem. A* **2001**, *105*, 3214–3220.
(24) Geuenich, D.; Hess, K.; Kohler, F.; Herges, R. *Chem. Rev.* **2005**, *105*, 3758–3772.
(25) Wolinski, K.; Hinton, J. F.; Pulay, P. *J. Am. Chem. Soc.* **1990**, *112*, 8251–8260.
(26) Keith, T. A.; Bader, R. F. W. *Chem. Phys. Lett.* **1993**, *210*, 223–231.
(27) Besides the standard optimization techniques, other methods used include eigenvector following searches, constrained optimizations, and multidimensional scans.

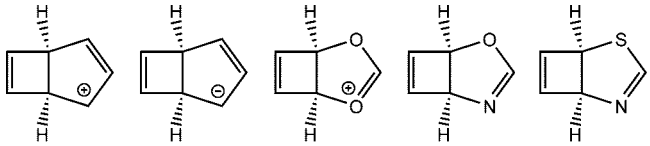

1a **1b** **1c** **1d** **1e**

FIGURE 3. Complexity increases in the backbone of the fused cyclobutenes from **1a** to **1e** to isolate the effects of backbone heteroatoms in the thermal-electrocyclic ring opening of **1h**.

TABLE 1. Relative Free Energies for the Electrocyclic Rearrangement of Molecules 1a−1e (in kcal/mol, 298 K)

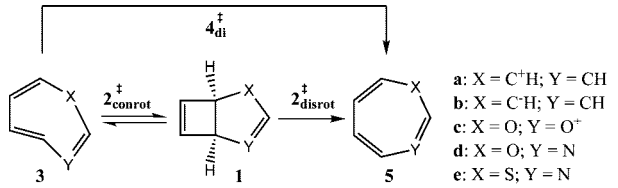

	a	b	c	d	e
			Disrotatory Opening		
1	0.0	0.0	0.0	0.0	0.0
$\mathbf{2}^{\ddagger}_{\text{disrot}}$	42.2	4.6	53.3	37.3	32.0
5	−52.9	−31.8	2.2	−11.8	−11.0
			Conrotatory Opening		
1	0.0	0.0	0.0	0.0	0.0
$\mathbf{2}^{\ddagger}_{\text{conrot}}$	16.6	−	50.5	36.5	30.4
3	7.6	−	45.5	32.6	23.9
$\mathbf{4}^{\ddagger}_{\text{di}}$	20.1	−	52.2	−	−
5	−52.9	−31.8	2.2	−11.8	−11.0

simplest model of **1h**, displays both dis- and conrotatory pathways. The W−H allowed transition state, with a barrier of 16.65 kcal/mol, yields a *Z*,*E*-cyclic intermediate **3a**, which undergoes *E*→*Z* isomerization through a rate limiting transition state of 20.13 kcal/mol. This two step reaction mechanism furnishes the final tropylium ion **5a**, which shows its inherent aromatic stability at 52.88 kcal/mol lower in energy than the initial product. The alternative disrotatory transition state $\mathbf{2a}^{\ddagger}_{\text{disrot}}$ was located via symmetry constrains. After imposing σ symmetry on the system, a second-order saddle point was located. This structure lies very high in energy at 42.19 kcal/mol compared with its W−H counterpart, rendering this rotatory alternative noncompetitive.

The anionic model **1b**, in contrast, is shown to undergo a symmetry-forbidden disrotatory ring opening via a very low energy transition state $\mathbf{2b}^{\ddagger}_{\text{disrot}}$ at 4.58 kcal/mol. This behavior is seemingly due to the cyclopentenyl anion moiety showing very strong bias toward its allowed six-electron disrotatory ring opening, overriding the symmetry requirements of the cyclobutene ring opening. Moreover, the large excess of electronic density in the five-membered ring is likely to flow into the cyclobutene moiety at the transition state, thus alleviating much of the energy penalty associated with the four-electron disrotatory ring opening (vide infra). The strong repulsions due to the allyl anion in the rigid and compact fused reactant could also be responsible for such a mild activation barrier. Charge stabilization in the cycloheptatrienyl anion, however, is not as effective as in the cationic counterpart due to the antiaromatic set of eight π electrons, and **5b** lies only 31.84 kcal/mol below the reactants.

Heteroatom substitutions were performed in a sequential way so that W−H forbidden disrotatory transition states could be located via symmetry constrains for at least one model. The symmetric dioxa-substituted **1c**, thus, was considered as the first heteroatom containing candidate. Despite the expected difficulties, this model exhibited two well-defined first-order transition states, $\mathbf{2c}^{\ddagger}_{\text{conrot}}$ and $\mathbf{2c}^{\ddagger}_{\text{disrot}}$, associated with a conrotatory and a disrotatory electrocyclic ring opening, respectively.[28] The W−H transition state $\mathbf{2c}^{\ddagger}_{\text{conrot}}$ is just 2.7 kcal/mol lower in energy than the disrotatory alternative. Moreover, the *Z*,*E*-cyclic intermediate **3c** undergoes double-bond isomerization via a rate limiting transition state (52.21 kcal/mol). Altogether, the conrotatory and the disrotatory pathways are separated by only 1 kcal/mol, thus, rendering both alternatives competitive under working thermal conditions. The energetic similarity between allowed and forbidden transition states suggests that appropriate heteroatom substitution might actually steer the reactivity toward a disrotatory thermal ring opening.

Introduction of nitrogen in the molecular backbone allowed for construction of neutral species. Aza/oxa substitution promoted a drastic reduction of the activation barrier (ca. 15 kcal/mol), closing the energy gap between both rotatory alternatives. The disrotatory transition state lies within 1 kcal/mol of the symmetry-allowed $\mathbf{2d}^{\ddagger}_{\text{conrot}}$. The only major difference in terms of reactivity is the lack of double-bond isomerization in the transition state. The introduction of nitrogen in the molecular scaffold imposes some asymmetry in the ring backbone bond lengths. This distortion displaces the disrotatory transition state in the potential energy surface, engulfing the *E*→*Z* isomerization saddle point. Thus, in terms of reactivity, the conrotatory transition state leads to an unproductive intermediate **3d** or **3e**, which is deemed to revert to reactants before proceeding to the final products via disrotation (see Figure 4). Sulfur substitution in **1e** further decreases the activation barriers to 30.38 kcal/mol for $\mathbf{2e}^{\ddagger}_{\text{conrot}}$ and 31.99 kcal/mol for $\mathbf{2e}^{\ddagger}_{\text{disrot}}$, but maintains the same competitive profile as the oxa analogue.

3.1.2. Electronic Properties. The aromaticity of the disrotatory and conrotatory transition states for the electrocyclic ring opening of **1a**−**1e** was explored through the NICS methodology. Chemical shifts were measured at points along an axis centered in the cyclobutene geometric center and perpendicular to its mean plane. The variation and magnitude of the chemical shift along this axis provided valuable information regarding the aromatic character of the cyclobutene ring opening transition state (see Figure 5).

In our earlier work with neutral molecules,[10] we showed how symmetry-forbidden transition states avoid the considerable energy penalty associated with an antiaromatic electronic structure by resorting to open-shell diradicaloid species. In these cases the NICS values shifted from clearly antiaromatic (30 to 20 ppm) to mildly antiaromatic or merely nonaromatic (10 to 3 ppm). In our present work, the same trends apply; however, this shift is much more pronounced in ionic species due to various factors. The symmetry-allowed cationic transition state $\mathbf{2a}^{\ddagger}_{\text{conrot}}$ displays mild aromaticity as expected, but we surprisingly found that its forbidden alternative also exhibits a similar degree of deshielding at the center of the ring. The large electron density depletion inherent to the positively charged system is probably responsible for its low in-plane shielding values (see Figure 6). The anionic hydrocarbon model proceeds through a very low energy disrotatory opening, which evidences the competition between the two moieties in this bicyclic structure — on the

(28) No symmetry constraints had to be imposed to locate these transition states.

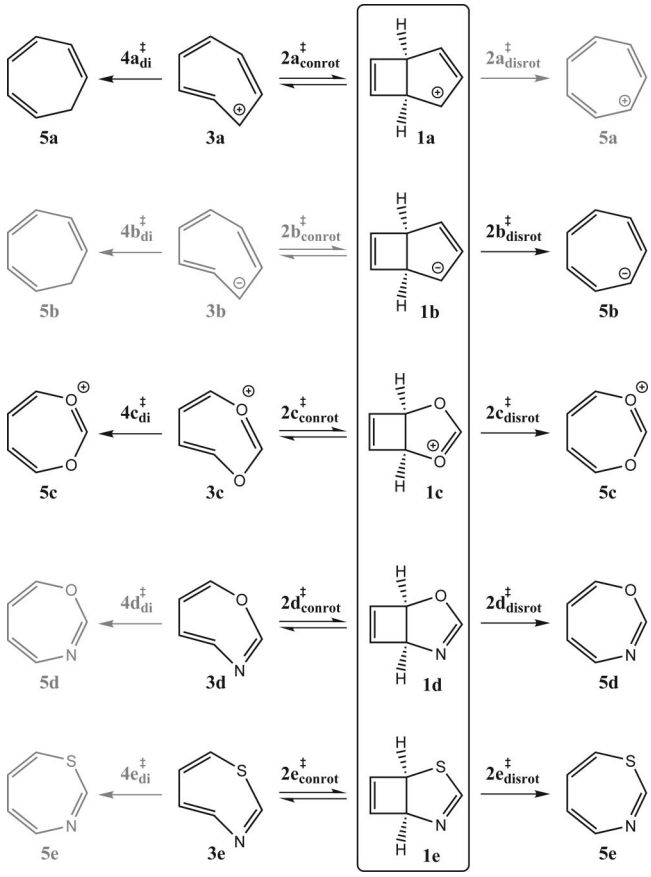

FIGURE 4. Implications of the potential energy surface on the reactivity of model compounds **1a**−**1e**. Grayed steps indicate non-occurring reactions.

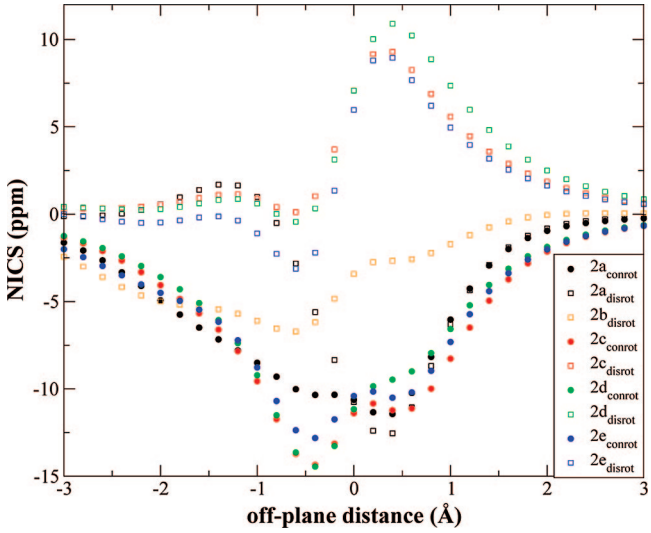

FIGURE 5. Nucleus independent chemical shifts computed along a perpendicular axis located at the geometric center of the four-membered ring at conrotatory and disrotatory ring opening transition structures of **1a**−**1e**. Conrotatory transition states are plotted with solid circles and their disrotatory counterparts are plotted with squares. Negative off-plane coordinates indicate points in the *endo* side of the bicyclic structure; conversely, positive values indicate points in the *exo* side of the molecule.

one hand, the disrotatory opening of the cyclobutene ring is a symmetry-forbidden process and should proceed via a high energy transition state; on the other hand, this opening is very

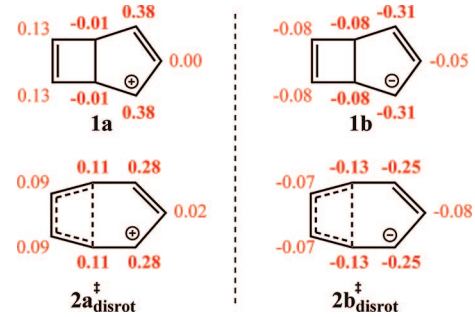

FIGURE 6. NBO partial charges in the hydrocarbon disrotatory transition states $\mathbf{2a}^{\ddagger}_{\text{disrot}}$ and $\mathbf{2b}^{\ddagger}_{\text{disrot}}$ compared to the reactants, **1a** and **1b**, respectively. Boldface numbers indicate changes larger than 0.05 electron.

favored for the cyclopentenyl anion half, which seems to strongly govern the whole process. This competition can be observed in terms of the NICS in Figure 5 with $\mathbf{2b}^{\ddagger}_{\text{disrot}}$ showing a very irregular (far from bell-shaped) deshielding along the off-plane axis. This interpretation is further reinforced by computing the NICS values along two axes centered at each fused ring. A destructive interaction was observed in the common *endo* region, and well-defined behavior expands in the divergent *exo* areas (see Supporting Information). The very low activation energy and the NICS plot suggest that the antiaromatic character of the four-electron disrotatory ring opening in the cyclobutene half has been somehow alleviated in the transition state. This interpretation seems plausible not only from energetic and magnetic grounds, but also from the reorganization of the electron density in the path from reactant to transition state. NBO charges indicate a large flow of electron density from the cyclopentenyl anion to the bridgehead carbon atoms in the transition state, likely increasing the electronic repulsions and deviating the cyclobutene moiety from the unstable four-electron state toward an electron richer state (see Figure 6).

Neutral and charge-localized model systems **1c**−**1e** adhered to the expected behavior in terms of the cyclobutane ring aromaticity. Conrotatory transition states exhibited two-maxima well-defined bell-shaped curves ranging from near zero NICS in points far away from the molecular plane to −12 ppm to −14 ppm for in-plane points. The two maxima at about 0.5 Å from the molecular plane are a typical signature for conrotatory transition states. Disrotatory transition states, in turn, showed evidence of moderate antiaromatic character with NICS values reaching 10 ppm. In line with the energy profiles for these reactions showing decreasing barriers for both the symmetry-allowed and forbidden ring opening steps, the diradical character of the disrotatory transition states decreased in the series OO **2c** > ON **2d** > SN **2e**,[29] suggesting an increased polar contribution to the transition state due to the lone pair donating/accepting abilities of the heteroatoms.

3.2. Substituents. The effect of substituents was taken into account also in a sequential approach starting from the unsubstituted model **1e**, the carboxylic acids at C6 and C7 **1f**, the amine group at C3 to build the isothiourea motif **1g**, and finally the experimental compound **1h** (see Figure 7).

Complete reaction profiles were computed for the ring opening of **1f**−**1h**. Using $\mathbf{2e}^{\ddagger}_{\text{conrot}}$ and $\mathbf{2e}^{\ddagger}_{\text{disrot}}$ as convenient templates, two sets of transition states were obtained for the series in Figure 7. The conrotatory transition state $\mathbf{2h}^{\ddagger}_{\text{conrot}}$ was

(29) S^2 values are 0.73, 0.51, and 0.00 for $\mathbf{2c}^{\ddagger}_{\text{disrot}}$, $\mathbf{2d}^{\ddagger}_{\text{disrot}}$, and $\mathbf{2e}^{\ddagger}_{\text{disrot}}$, respectively.

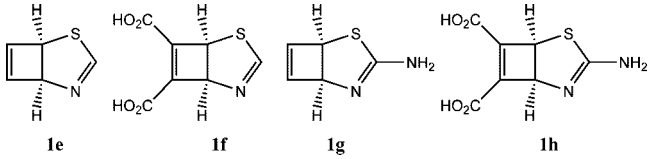

FIGURE 7. Set of molecules considered to explore the substituent effects in the thermal ring opening of **1h**.

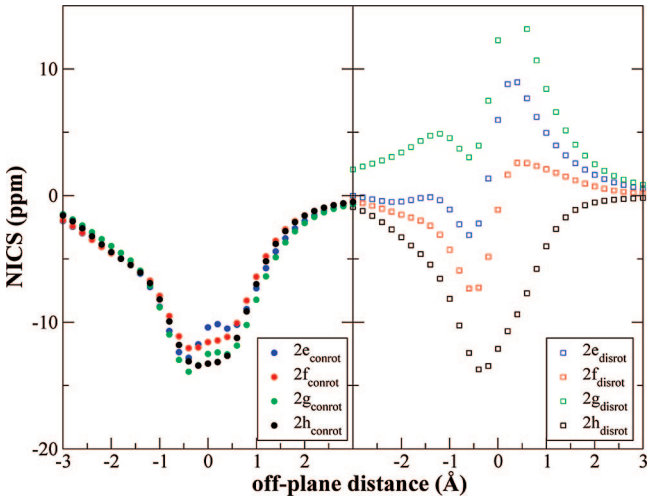

FIGURE 8. Nucleus independent chemical shifts computed along a perpendicular axis located at the geometric center of the four-membered ring at conrotatory and disrotatory ring opening transition structures of **1e**−**1h**. Conrotatory transition states were plotted with solid circles (left) whereas the disrotatory counterparts were plotted with squared symbols (right). Negative off-plane coordinates indicate points in the *endo* side of the bicyclic structure; conversely, positive values indicate points in the *exo* side of the molecule.

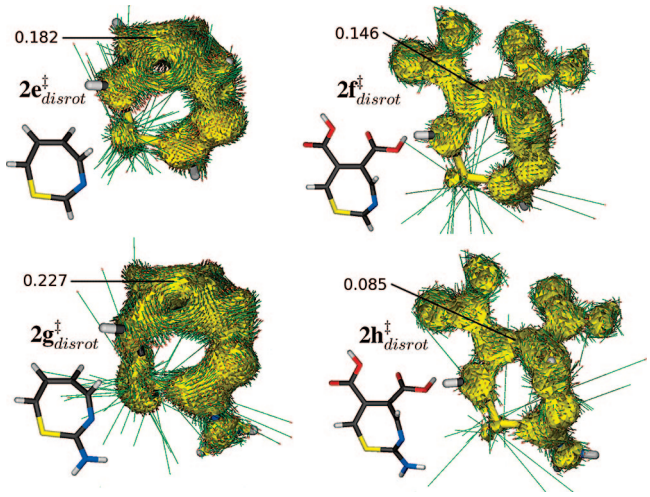

FIGURE 9. ACID (isosurface value 0.05 au) for transition states $\mathbf{2e}^{\ddagger}_{\text{disrot}}$−$\mathbf{2h}^{\ddagger}_{\text{disrot}}$ and critical isosurface values (CIV) at the C6−C7 bond.[31] The external magnetic field vector is perpendicular to the cyclobutene mean plane (the same axis used to compute the NICS values was employed to apply the external field).

compared to that reported in preceeding work,[11] characterized as a symmetry-forbidden disrotatory transition state, and was found to be identical. The conrotatory motion of $\mathbf{2h}^{\ddagger}_{\text{conrot}}$ was confirmed by IRC calculations (vide infra). We, nevertheless, located a seemingly disrotatory transition state, $\mathbf{2h}^{\ddagger}_{\text{disrot}}$, which kept open the possibility for a symmetry-forbidden ring opening in **1h**.

TABLE 2. Relative Free Energies for the Electrocyclic Rearrangement of Molecules 1e−1h (in kcal/mol, 298 K)

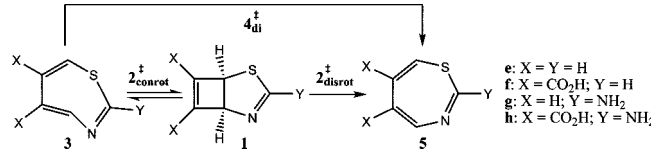

	e	f	g	h
	Disrotatory Opening			
1	0.0	0.0	0.0	0.0
$\mathbf{2}^{\ddagger}_{\text{disrot}}$	32.0	27.5	34.3	24.9
5	−11.0	−8.7	−14.1	−13.1
	Conrotatory Opening			
1	0.0	0.0	0.0	0.0
$\mathbf{2}^{\ddagger}_{\text{conrot}}$	30.4	26.5	29.4	24.7
3	23.9	20.6	24.6	20.7
$\mathbf{4}^{\ddagger}_{\text{di}}$	–	–	–	–
5	−11.0	−8.7	−14.1	−13.1

Table 2 summarizes the reaction profiles for the S/N series **1e**−**1h**. The energetics of the series made apparent strong substituent effects that, however, did not seem systematic. These effects were propagated along the transition states and the intermediate, but they were not clear in the final products. They, therefore, had kinetic impact, but did not compromise the stability of the final heterocycloheptatrienes. Both the conrotatory and the disrotatory transition states and the intermediate in the ring opening of **1f** were about 4 kcal/mol lower in energy than the corresponding stationary point for **1e**. This energy reduction was lost in **1g**; actually, the disrotatory transition state $\mathbf{2g}^{\ddagger}_{\text{disrot}}$ was higher in energy than the unsubstituted system. The introduction of both the electron-withdrawing carboxylic acid and the electron-donor amine seemed to produce a synergistic push−pull effect, also called captodative effect or merostabilization,[30] to lower the activation energies further than the amine group alone (see entries **f** and **h** in Table 2).

The aromatic properties of these transition structures were also explored through the NICS methodology, and the results are summarized in Figure 8. The NICS curves for the symmetry-allowed transition states display the expected features with smooth, bell-shaped curves, reaching typical values of moderate aromatic character (−12 to −14 ppm) and showing very little variation with respect to the exocyclic substituents. On the contrary, the disrotatory transition states exhibited a very wide variability depending on the substituents located in the periphery of the molecular scaffold. The actual dependence was very surprising and nonlinear — the simplest, unsubstituted model, $\mathbf{2e}^{\ddagger}_{\text{disrot}}$, showed very mild antiaromatic features; addition of the carboxylic acids at C6 and C7 seemed to deactivate the destabilizing four-electron cyclic motif via their strong electron-withdrawing nature, thus, canceling the antiaromatic characteristics (see $\mathbf{2f}^{\ddagger}_{\text{disrot}}$, Figure 8). The inclusion of the amine group induced the opposite effect, and $\mathbf{2g}^{\ddagger}_{\text{disrot}}$ presented stronger antiaromaticity than the parent system. Surprisingly, the addition of both the carboxylic acids and the amine group in **2h**, instead of a destructive interference, displayed a synergistic effect inverting the antiaromatic character enhancement of the amine group. This dramatic switch in the magnetic properties suggests that a specific interaction occurs only when electron-withdrawing and electron-donating groups are found in the molecular structure at C6−C7 and C3, respectively.

(30) Bordwell, F. G.; Lynch, T.-Y. *J. Am. Chem. Soc.* **1989**, *111*, 7558–7562.

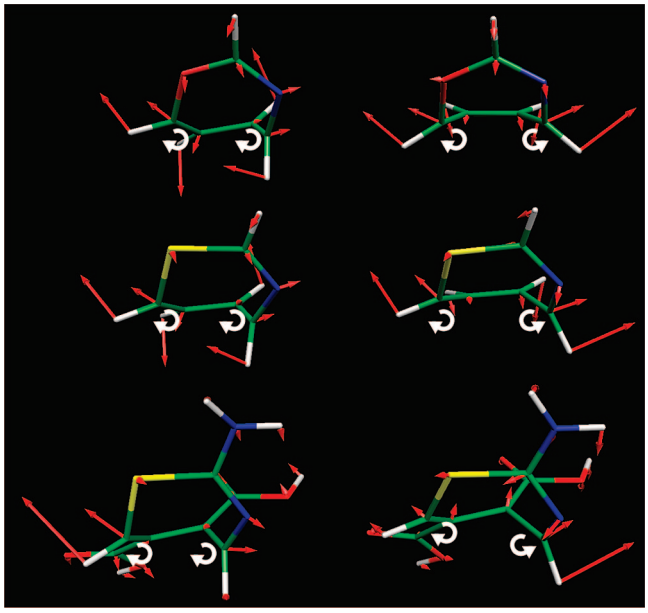

FIGURE 10. Displacement vectors of the normal mode associated with the imaginary frequency in transition states $\mathbf{2d}^{\ddagger}_{\text{conrot}}$, $\mathbf{2e}^{\ddagger}_{\text{conrot}}$, and $\mathbf{2h}^{\ddagger}_{\text{conrot}}$ (left) and $\mathbf{2d}^{\ddagger}_{\text{disrot}}$, $\mathbf{2e}^{\ddagger}_{\text{disrot}}$, and $\mathbf{2h}^{\ddagger}_{\text{disrot}}$ (right). The white arrows indicate the rotatory direction in each case.

Ⓦ Movies for the full reaction path computed are provided for $\mathbf{2e}^{\ddagger}_{\text{conrot}}$, $\mathbf{2e}^{\ddagger}_{\text{disrot}}$, $\mathbf{2h}^{\ddagger}_{\text{conrot}}$, and $\mathbf{2h}^{\ddagger}_{\text{disrot}}$.

To further confirm the conclusions derived from the NICS values, we computed the ACID. Figure 9 shows the delocalized density at the transition states $\mathbf{2e}^{\ddagger}_{\text{disrot}}$, $\mathbf{2f}^{\ddagger}_{\text{disrot}}$, $\mathbf{2g}^{\ddagger}_{\text{disrot}}$, and $\mathbf{2h}^{\ddagger}_{\text{disrot}}$ and the vector field indicating the density current direction. Delocalized density and current direction show good agreement with the interpretation of the NICS values — the model system $\mathbf{2e}^{\ddagger}_{\text{disrot}}$ displays a mild antiaromatic ring current located at the opening cyclobutene moiety; inclusion of the carboxylic acid groups in $\mathbf{2f}^{\ddagger}_{\text{disrot}}$ drastically deactivates the cyclobutene ring, disrupting the antiaromatic current; on the contrary, the amine group in $\mathbf{2g}^{\ddagger}_{\text{disrot}}$ injects electron density in the bicyclic system strengthening the paramagnetic ring current; finally, the introduction of both electron-donor and acceptor groups in $\mathbf{2h}^{\ddagger}_{\text{disrot}}$, instead of creating a balance in terms of electron density donated to/withdrawn from the bicyclic scaffold, drastically reduce the delocalized density and cancels the antiaromatic ring current.

Given such drastic changes in the electronic properties of the system due to the presence of both the carboxylic acids and the amine, we decided to explore whether there are chemical consequences derived from them. We focused in the first and last models in our series, $\mathbf{2e}^{\ddagger}_{\text{disrot}}$ and $\mathbf{2h}^{\ddagger}_{\text{disrot}}$. In terms of geometry, structures for transition states $\mathbf{2e}^{\ddagger}_{\text{disrot}}$–$\mathbf{2h}^{\ddagger}_{\text{disrot}}$ are similar, the main differences being small distortions in the cyclobutene moiety due to steric contacts between the carboxylic acids. In terms of the normal modes associated with the reaction coordinate, however, some differences arise that correlate well with the observations. Figure 10 illustrates the displacement vectors of the reaction coordinate normal mode for transition associated with the ring opening of **1d**, **1e**, and **1h**. The clear-cut conrotatory and disrotatory transition structures $\mathbf{2d}^{\ddagger}_{\text{conrot}}$ and $\mathbf{2d}^{\ddagger}_{\text{disrot}}$ serve as useful models for comparison purposes. Careful inspection of Figure 10 reveals that the geometry and displacement vectors are weakly affected by substitution. The main perturbation in terms of geometry is due to the longer C–S bonds compared to the C–O bond. On the other hand, the main difference in terms of displacement vectors is the motionless hydrogen geminal to the nitrogen in $\mathbf{2h}^{\ddagger}_{\text{conrot}}$. This apparent stillness of a hydrogen that should supposedly rotate along the reaction pathway is due to the transition state being slightly more advanced in $\mathbf{2h}^{\ddagger}_{\text{conrot}}$, occurring at a reaction coordinate where this hydrogen already underwent most of its motion. This characteristic makes the task of discerning the conrotation/disrotation alternatives more challenging from the mere observation of the stationary point. Disrotatory transition states, on the other side, exhibit somehow larger distortions of less clear origin[32] and pronounced variations in the displacement vectors. From the very symmetric vector arrangement in $\mathbf{2d}^{\ddagger}_{\text{disrot}}$, the introduction of sulfur imposes some degree of twist in the bicyclic backbone which reduces the vibrational motion of C=C–S fragment of the cyclobutene. Transition state $\mathbf{2h}^{\ddagger}_{\text{disrot}}$ is further twisted, which reduces significantly the vibrational motion of the C=C–S fragment of the cyclobutene, whereas the other fragment keeps a high degree of rotation.

All the analyses performed in these systems revealed striking differences in the series of disrotatory transition states. Particularly, the analysis of the displacement vectors associated with the normal mode with imaginary frequency suggests that the chemical reaction involving these transition states might actually be different. We, therefore, decided to perform intrinsic reaction coordinate calculations for $\mathbf{2e}^{\ddagger}_{\text{disrot}}$ and $\mathbf{2h}^{\ddagger}_{\text{disrot}}$. Surprisingly, the IRC calculations revealed that, despite the fairly similar energetics and geometry, $\mathbf{2e}^{\ddagger}_{\text{disrot}}$ and $\mathbf{2h}^{\ddagger}_{\text{disrot}}$ connect different kinds of minima. Transition state $\mathbf{2e}^{\ddagger}_{\text{disrot}}$ connects, as expected, **1e** and **5e** through a disrotatory process, but $\mathbf{2h}^{\ddagger}_{\text{disrot}}$ undergoes a monorotatory process by which an *E*→*Z* double-bond isomerization is completed. Therefore, transition state $\mathbf{2h}^{\ddagger}_{\text{disrot}}$ corresponds not to a disrotatory process, but to a double-bond isomerization process (movies for the full reaction path computed are provided in the online version of this paper for $\mathbf{2e}^{\ddagger}_{\text{conrot}}$, $\mathbf{2e}^{\ddagger}_{\text{disrot}}$, $\mathbf{2h}^{\ddagger}_{\text{conrot}}$, and $\mathbf{2h}^{\ddagger}_{\text{disrot}}$). Close inspection of the latter IRC ($\mathbf{2h}^{\ddagger}_{\text{disrot}}$) revealed some of the features that make the distinction between disrotation and direct isomerization unusually challenging for this substrate. The direct isomerization process is expected to involve mainly rotations about the isomerizing double-bond; however, in $\mathbf{2h}^{\ddagger}_{\text{disrot}}$ this transformation is coupled with considerable motion of the C=C–S moiety. Actually, in early steps of the isomerization, the motion can be interpreted as a fairly clear conrotation until the proximities of the transition state, where the C=C–S part *bounces* backward and resembles a disrotatory opening. It is not until the latter stages of the IRC where the eventual double-bond isomerization becomes clear. Structures switching character along the reaction coordinate have been reported for electrocyclic ring opening reactions of small fused rings.[4] IRC calculations performed on the remaining transition states in Table 2 also provided similar conclusions — transition states showing strong electronic evidence of antiaromatic behavior are indeed disrotations ($\mathbf{2g}^{\ddagger}_{\text{disrot}}$), whereas, electron-deficient transition structures correspond to double-bond isomerization processes ($\mathbf{2f}^{\ddagger}_{\text{disrot}}$). Conrotatory transition states, on the contrary, are always located, are largely unaffected by

(31) Critical isosurface values (CIV) indicate the value of the ACID scalar field at the junction of delocalization densities from different groups of atoms. This point is to the ACID what the ring critical point is to the electron density in the AIM analysis (see ref 24 for a more detailed definition).

(32) The geometry differences between $\mathbf{2d}^{\ddagger}_{\text{disrot}}$ and $\mathbf{2e}^{\ddagger}_{\text{disrot}}$ are mostly due to longer S–C bonds, but unlike in the conrotatory transition states, the introduction of the amine and carboxylic groups impacts the geometry of $\mathbf{2h}^{\ddagger}_{\text{disrot}}$ significantly, resulting in a late transition state.

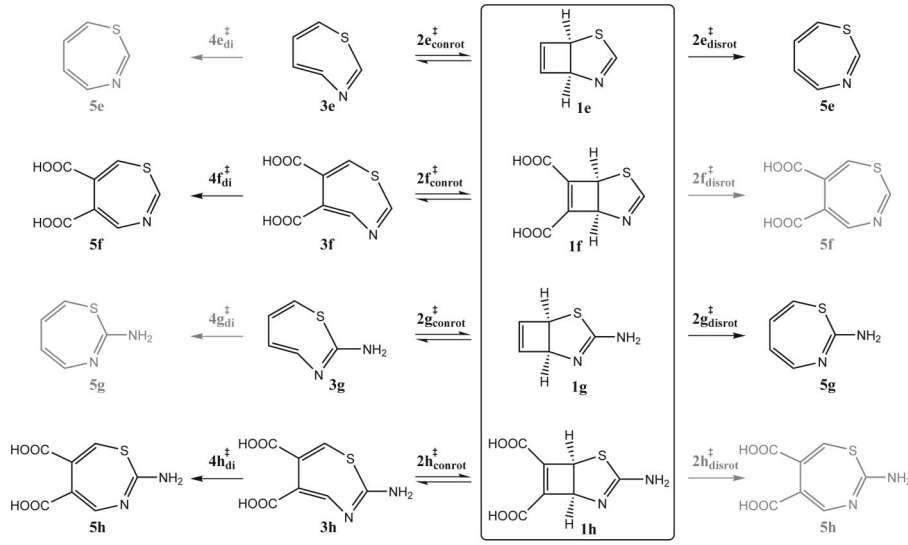

FIGURE 11. Implications of the substituents in the electrocyclic ring opening mechanism of 2-thia-4-azabicyclo[3.2.0]heptadienes, **1e**−**1h**.

TABLE 3. Relative Free Energies for the Electrocyclic Rearrangement of Molecules 1e−1h (in kcal/mol, 298 K)

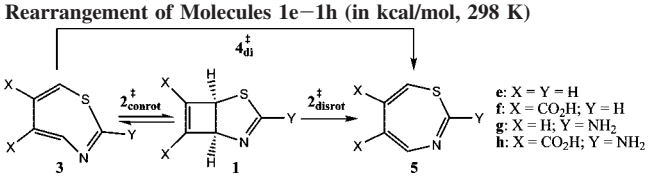

	e	f	g	h
		Disrotatory Opening		
1	0.0	0.0	0.0	0.0
$\mathbf{2}^{\ddagger}_{\text{disrot}}$	32.0	−	34.3	−
5	−11.0	−8.7	−14.1	−13.1
		Conrotatory Opening		
1	0.0	0.0	0.0	0.0
$\mathbf{2}^{\ddagger}_{\text{conrot}}$	30.4	26.5	29.4	24.7
3	23.9	20.6	24.6	20.7
$\mathbf{4}^{\ddagger}_{\text{di}}$	−	27.5	−	24.9
5	−11.0	−8.7	−14.1	−13.1

substitution, and are the lowest energy pathways of the two alternatives when this alternative exists.

Therefore, Table 2 has to be reorganized to reflect the latter findings in terms of which reactant−product pair each transition state connects. Table 3 summarizes the final mechanistic picture for the S/N series of molecules **1e**−**1h**. Interestingly, the implications of exocyclic substitution in the mechanistic landscape of the ring opening reactions across Figure 7 are major. For systems **1e** and **1g** no double-bond isomerization transition state was found. The result was a conrotatory ring opening process leading to unproductive intermediates **3e** and **3g**, respectively, which, in close analogy to **3d** (vide supra), were deemed to revert to reactants before proceeding to the final producs via the alternative disrotatory transition states $\mathbf{2e}^{\ddagger}_{\text{disrot}}$ and $\mathbf{2g}^{\ddagger}_{\text{disrot}}$. On the contrary, for systems sporting the carboxylic acid groups, the disrotatory transition states could not be located, which reduced the mechanistic probabilities to a single sequential pathway starting with conrotatory ring opening followed by *E*→*Z* double-bond isomerization. All these reactivity implications are summarized as reaction equations in Figure 11.

It is interesting how strongly exocyclic substituents affect the reactivity of this fused cyclobutene motif. By a careful selection of substituents, the reaction can be steered through the allowed conrotatory ring opening (due to the disrotatory alternative being higher in energy or nonexistent) or through the forbidden disrotatory ring opening (due to the conrotatory alternative being an unproductive pathway). Both mechanistic alternatives have no effect on the final product of the reaction but show the close competition that W−H and anti-W−H reactions can achieve for some substrates. Furthermore, the aromaticity of the transition structures is strongly affected by the character of the groups attached to it and by the interference effects between these groups.

4. Conclusions

Regardless of the nature of the heteroatoms at positions 2 and 4 of the bicyclo[3.2.0]hepta-3,6-diene core, their electrocyclic ring opening reactions are predicted to follow the W−H allowed conrotatory pathway leading finally to the corresponding heterocyclic system **5** with *cis*,*cis*,*cis* geometry after double-bond isomerization of the *cis,cis,trans*-isomer **3**. In some cases, the competing electrocyclic ring closure of the high energy intermediate **3** makes feasible a reaction course through the disfavored disrotatory path. Strong electron-donating (NH_2 at C3) and electron-withdrawing (CO_2H at both C6 and C7) substituents drastically altered the energy profile landscape of the two mechanistic alternatives that are so close in geometry and energy. In particular, for analogues with sulfur and nitrogen at positions 2 and 4 of the bicyclic motif, the disrotatory and double-bond isomerization transition states collapsed into a single saddle point which connects reactant **1** and product **5** (via disrotation) or intermediate **3** and product **5** (via double-bond isomerization), depending on the electronic nature of the substituents adorning the molecular skeleton. Therefore, care needs to be taken on the analysis aimed to interpret and identify transition states in the anti-W−H/diradical realm.

Acknowledgment. The authors are grateful to the Centro de Supercomputación de Galicia (CESGA) for allocation of computation time. C.S.L. is grateful to the Xunta de Galicia for financial support through the Isidro Parga Pondal program.

Supporting Information Available: Cartesian coordinates, SCF energies, number of imaginary frequencies for each structure. This material is available free of charge via the Internet at http://pubs.acs.org.

JO802678D